Article:

Reid, L., Thougaard, J., Price, O.J. orcid.org/0000-0001-8596-4949 et al. (3 more authors) (2024) Application of computational fluid dynamics to investigate pathophysiological mechanisms in exercise-induced laryngeal obstruction. Journal of Applied Physiology, 137 (4). pp. 984-994. ISSN 8750-7587

https://doi.org/10.1152/japplphysiol.00230.2024

RESEARCH ARTICLE

RUNNING HEAD: Investigating EILO using Computational Fluid Dynamics

Application of computational fluid dynamics to investigate pathophysiological mechanisms in exercise-induced laryngeal obstruction

Reid L[1,2], Thougaard J[3], Price OJ[4,5], Hayatdavoodi M[2], Pedersen L[3], Walsted E[3].

[1] Brighton and Sussex Medical School, University of Sussex, England, BN1 9PX, UK

[2] School of Science and Engineering, University of Dundee, Scotland, DD1 4HN, UK

[3] Department of Respiratory and Infectious Diseases, Bispebjerg Hospital, Copenhagen, Denmark

[4] School of Biomedical Sciences, Faculty of Biological Sciences, University of Leeds, UK

[5] Department of Respiratory Medicine, Leeds Teaching Hospitals NHS Trust, UK

Correspondence: Dr. Emil Walsted (emilwalsted@dadlnet.dk), Respiratory Research Unit, Department of Respiratory Medicine, Bispebjerg Hospital, Bispebjerg Bakke 23, 2400 Copenhagen NV

ABSTRACT

The underlying pathophysiological mechanisms of exercise-induced laryngeal obstruction (EILO) remain to be fully established. It is hypothesised that high inspiratory flow rates can exert a force on laryngeal airway wall that contribute to its inward collapse causing obstruction. Computational fluid dynamics (CFD) presents an opportunity to explore the distribution of forces in a patient specific upper airway geometry. The current study combined exercise physiological data and CFD simulation to explore differences in airflow and force distribution between an EILO patient and a healthy-matched control. participants underwent incremental exercise testing with continuous recording of respiratory airflow and laryngoscopic video, followed by an MRI scan. The respiratory and MRI data were used to generate a subject specific CFD model of upper respiratory airflow. In the EILO patient, the posterior supraglottis experiences an inwardly directed net force, whose magnitude increases nonlinearly with larger flow rates, with slight changes in the direction toward the centre of the airway. The control demonstrated an outwardly directed force at all regions of the wall, with a magnitude that increases linearly with larger flow rates. A comparison is made between the CFD results and endoscopic visualisation of supraglottic collapse, and very good agreement is found. The current study presents the first hybrid physiological and computational approach to investigate the pathophysiological mechanisms of EILO, with preliminary findings showing great potential, but should be utilised in larger sample sizes to confirm findings.

NEW & NOTEWORTHY

The current study is the first to use a hybrid combined computational fluid dynamics and exercise physiology approach to investigate pathophysiology in EILO. The hybrid methodology is a promising approach to explore the pathophysiological mechanisms underlying the condition. Notable differences occur in the distribution of airflow and wall forces between the EILO and control participants, which align with symptoms and visual observations.

Keywords:

Exercise-induced laryngeal obstruction; EILO; Computational Fluid Dynamics; Dyspnoea; CFD; aerodynamic forces.

INTRODUCTION

Exercise-induced laryngeal obstruction (EILO) is a condition characterised by temporary closure of the laryngeal inlet (i.e., glottic +/- supraglottic structures) that precipitates breathlessness, cough, and inspiratory stridor on exertion [1-3]. The global prevalence of EILO remains to be fully established, however observational and field-based studies conducted over the past decade indicate that up to 5-7% of adolescents and young adults are affected [4-6], with a particularly high incidence in females (76%) and athletic individuals undertaking endurance-based sport (35.2%) [7-9]. It is also now recognised that EILO co-exists in a significant proportion (>30%) of people with pre-existing chronic obstructive airways disease (e.g., asthma and COPD) reporting activity-related breathlessness and high symptom burden [8-13].

The pathophysiological mechanisms of EILO are still under investigation, however, insufficient mechanical resistance of laryngeal tissues to aerodynamic forces during inspiration has been hypothesised [1,9]. Walsted et al. [14] studied onset of laryngeal closure, breathing pattern, and neural respiratory drive

(NRD) in EILO patients to provide insight into the pathophysiological mechanisms underlying the condition. It was identified that at lower work rates, although no differences were seen in work of breathing or NRD, EILO patients had a greater tidal volume, and therefore greater minute ventilation, compared to the healthy matched controls. This ventilatory pattern persisted throughout the exercise test, where pronounced differences in work of breathing and NRD became apparent at high intensity work rates.

In adult and adolescent populations, there is a preponderance for EILO towards females. Interestingly, this is not observed in prepubescent populations where the gender distribution seems to be comparable [1,4-8]. This difference may be attributed to the sex-based differences in laryngeal growth during puberty, leading to male thyroid cartilages being taller with larger anterior-posterior diameters, and a more acute thyroid angle in comparison to females. The consequence of this precipitates males having a longer and narrower laryngeal airway, which is known to impact vocalisation [15]. These anatomical differences and their correlation with inspiratory airflow are yet to be explored, which may contribute to the pathophysiological mechanisms underlying EILO.

Computational fluid dynamics (CFD) is an *in-silico* approach for studying fluid motion that has previously been applied to upper respiratory tract (URT) pathologies, such as obstructive sleep apnea [16] and tracheomalacia [17]. CFD offers the opportunity to study the upper airway and obtain data that are unavailable in clinical scenarios in a safe and variable controlled manner. Indeed, previous research evaluating inspiratory airflow has identified that flow rate and airway geometry can alter the airflow and supraglottic wall pressures in high inspiratory flow that may contribute to the closure observed clinically [18,19]. Specifically, Reid et al. [18] identified that steady inspiratory flow rates larger than 120 L/min alter the pressure distribution in the supraglottic airway and at the airway walls [19]. Specific geometric features of hypopharyngeal and laryngeal airway, such as the piriform fossae and epiglottis, appear to have a profound impact on the distribution of airflow in the laryngeal airway at high inspiratory flow rates [19]. CFD has also been used to investigate the various altered breathing patterns used in the conservative treatment of EILO and their influence on downstream airflow at the larynx [20]. However, there are currently no studies using CFD in conjunction with real patient data to explore and better understand the pathophysiological mechanisms underlying EILO.

The current study aims to explore an approach to investigate the pathophysiological mechanisms of EILO by combining the CFD approach with imaging and physiological data obtained from an EILO patient and a healthy control. This was achieved through: (1) assessment of the velocity and pressure changes in URT airflow throughout incremental exercise testing; (2) establishing the magnitude and direction of air-induced force acting on the glottic and supraglottic walls; and (3) comparing these findings between an EILO patient and a healthy control with accompanying laryngoscopic observations.

MATERIALS AND METHODS

Participants

For a comparative and illustrative analysis, the recruitment included one patient with EILO and one healthy control (matched for age, sex and BMI) from the respiratory outpatient clinic at Bispebjerg Hospital, Copenhagen, Denmark. Subject demographics are detailed in Table 1. Written informed consent was obtained from both participants and the study was approved by the Regional Ethics Committee in the Capital Region in Denmark (H-20057391, amendment 95273).

Table 1. Subject demographics

	EILO	Control
Age, years	45	46
Sex	Female	Female
Height, cm	171.5	150
Weight, kg	66.5	50
Body mass index, kg/m^2	22.6	22.2
FEV_1, L (% predicted)	2.80 (87%)	2.64 (99%)
FVC, L (% predicted)	3.76 (93%)	3.34 (101%)
FEV_1/FVC	0.74	0.79
Peak work rate, Watts	214	190

Continuous laryngoscopy during exercise (CLE) test protocol

The participants underwent an incremental exercise test to volitional maximal effort on a bicycle ergometer (Corival CPET; Lode, Groningen, the Netherlands) with continuous recording of airflow (HR-800L pneumotach, Hans Rudolph, Kansas City, USA) and laryngoscopic video (ENF-V2, Olympus, Tokyo, Japan). Following a 5-minute light warmup at 50 Watts (W), the participants exercised at initially 100 W with increments of 2 W every 6 seconds [21]. EILO was diagnosed via continuous laryngoscopy during exercise (gold-standard approach to detection) during clinical workup in accordance with international guidance. The laryngoscopic video was analysed and rated by two independent experts, grading the severity of closure at both the glottic and supraglottic levels as none, mild, moderate or severe (0–3) as per the widely used Norwegian EILO grade scoring system.

Data recording and processing

Laryngoscopic video and airflow-/volume data were recorded via a multi-purpose data recording system (PowerLab 16/35, AD-instruments, Sydney, Australia) using LabChart version: 8.1.16. Perceived dyspnoea and leg discomfort were manually recorded, using a modified Borg (1-10), scale at baseline (post-warmup) and every minute throughout the test, and immediately post-test. Volume was corrected to body temperature pressure saturated (BTPS) volume. Respiratory physiology parameters were calculated using custom developed Python-based software (RespMech 1.0, www.respmech.dk, DOI: 10.5281/zenodo.3270825).

Computational fluid dynamics model

Imaging and 3-D Reconstruction

Static imaging of the URT was acquired in both participants through magnetic resonance (MR) imaging. T1 MR images were obtained using a SIEMENS MAGNETON 3.0T XT Numaris scanner at Bispebjerg Hospital, Copenhagen, Denmark. Images were obtained in the axial plane with a resolution 0.4 x 0.4 mm^2 and slice thickness of 3.0 mm. Three-dimensional geometry of the URT was reconstructed using the 3DSlicer software package (Version 5.0.3). MRI scan data of both participants were initially segmented using thresholding with any artefacts being manually edited to achieve an accurate geometry. The 3D reconstructions were reviewed by an experienced clinician. The reconstructions were imported into Blender (Version 2.83.0) to establish the inlet and outlet, and any necessary smoothing surface elements that may impact modelling procedure. The final geometries are demonstrated in Figure 1.

Cross-sections and regions of interest

Figure 1 presents all cross-sections and regions of interest in both participants. Six equally spaced horizontal cross-sections (A-A′ to F-F′) through between the epiglottic constriction and the glottis were established to capture airflow in the supraglottic and hypopharyngeal regions. To analyse the air-induced loads on the hypopharyngeal and laryngeal walls, sixteen regions of interest were defined. The glottic wall was divided into eight regions of interest, with four regions on each of the right and left sides. These glottic regions are equally spaced between the anterior commissure and the posterior limit of the vocal fold, as shown in Figure 1(e). The eight regions of the supraglottic wall, with four on each side, consist of the surface extending from the internal vestibular fold over the aryepiglottic fold towards the inferior limit of the external piriform fossa. The supraglottic regions are equally spaced in the anterior-posterior direction along the laryngeal inlet, see Figure 1(e).

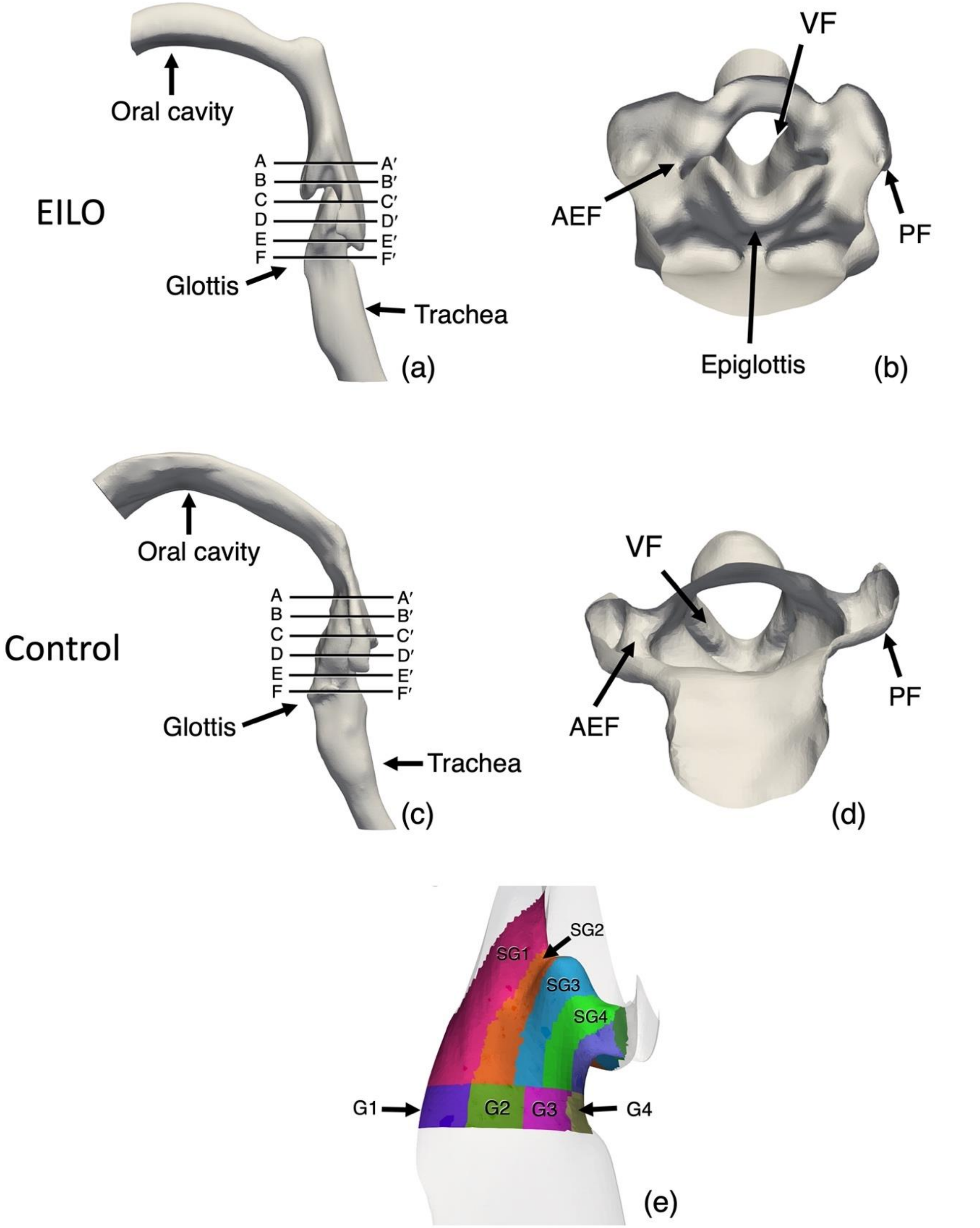

Figure 1. (a,c) left lateral and (b,d) superior views of EILO (top row) and control subject (middle row) geometries, respectively. Axial cross-sections A-A′ to F-F′ for EILO and control participants are shown in (a) and (c), respectively. (e) A midsagittal cross-section demonstrating four supraglottic and four glottic regions of interest in the EILO subject. VF, Vocal fold; AEF, Aryepiglottic fold; PF, Piriform fossa.

Computational fluid dynamics analysis

A CFD approach was used to model airflow through the URT and obtain aerodynamic loads exerted on the airway wall at physiological inspiratory flow rates. Assuming air is homogeneous and incompressible, for the velocities of interest to this study, the flow was governed by the Reynold-averaged Navier-Stoke (RANS) equations, discussed in the Appendix. Viscous effects were captured by use of the standard k-ω turbulence model [22] to simulate steady, uniform inspiratory airflow through the URT. It was shown by Mylavarapu et al. [23] that a k-ω model is suitable to study the airflow in the laryngeal airway. A series of simulations were conducted using respiratory data obtained during the CLE-test. The average peak inspiratory flow rates obtained using the respiratory data for each minute the participants performed the incremental CLE-test were used as drive airflow (Table 2). The no-slip condition was applied to the walls, a fixed pressure of 0 cmH2O at the outlet (trachea) and at the inlet (mouth) a steady, uniform volumetric flow rate was applied for each simulation. The model used in this study has been validated and verified by use of laboratory experiments and in-silico data, see Reid et al. [18]. For the computation discretization, a similar mesh was used to that developed by Reid et al. [18]. Further details on the numerical model are provided in the Appendix. Normalised velocity ($U_{norm} = U/U_{inlet}$) was used to investigate the distribution of velocity throughout the URT, where *U is* velocity and U_{inlet} is the inlet velocity. Airflow velocity was normalised against the prescribed inlet velocity for each simulation. Force over glottic and supraglottic regions of interest were obtained by integrating pressure over the specified regions of interest.

Table 2. Average peak inspiratory flow rate (Q) during each minute of exercise.

CLE test period (min)	**EILO (L/min)**	**Control (L/min)**
1	100.00	117.0
2	112.5	130.0
3	132.3	164.5
4	144.8	-
5	182.6	-
Identical Q	164.5	164.5

RESULTS

Analysis of velocity and pressure field

Normalised flow velocity contours through the URT and axial cross-sections at the final minute of the CLE-test for both participants (minute 5 – EILO; minute 3 – control) are summarised in Figure 2. Airflow in the EILO subject shows a higher velocity stream in the posterior regions of the URT that increases at the epiglottic and glottic constrictions, see Figure 2(a). The regions of high velocity flow through the larynx are relatively broad in the anterior-posterior dimension, with slower velocity magnitudes are seen at the anterior supraglottic region (cross-sections B-B′ and C-C′). These slower velocity magnitudes correspond to recirculation zones observed downstream of the epiglottic region. At the glottis, velocity significantly increases due to formation of the well-documented glottic jet, which extends downstream into the tracheal airway. The control subject demonstrates a different pattern of velocity distribution with higher normalised velocities observed at the epiglottic and glottic jets that are contiguous and continue into the posterior trachea. A comparison of the velocity distribution across the minutes of the CLE-test demonstrated high levels of consistency and remained invariant with increased flow rate in both participants. However, as expected, the velocity magnitude increases with higher flow rates applied to the inlet, shown in Figure 5(a-b).

Figures 3 and 4 present the pressure field contours corresponding to each minute of the CLE-test for the EILO and control participants, respectively. Importantly, the pressures shown in Figures 3 and 4 demonstrate *changes* in pressure as airflow passes towards the tracheal outlet and not absolute pressure values. In both participants, the cross-sectional pressure distribution in the hypopharyngeal and laryngeal airway is non-uniform. Figure 3 presents the pressure field for the EILO subject for each minute of the CLE-test which demonstrates a clear pressure drop from the mouth to the inferior portions of the trachea. Comparison across the minutes of the CLE-test outline variations in pressure distribution in the hypopharyngeal and laryngeal regions, shown in the cross-sections of Figure 3(a-e). Cross-sections C-C′ to F-F′ show an accumulation of pressure in the piriform fossae and a pressure reduction in lower supraglottic and glottic airway. In the control subject, the pressure distribution is remarkably different due to pressure remaining positive in all areas of the URT, except in the inferior trachea and small region in the posterior supraglottis, shown in Figure 4. A similar pattern of increasing pressure occurs in the piriform fossa, but regions of higher pressure are observed in the lateral regions of the supraglottic airway, shown in cross-sections C-C′ and D-D′ of Figure 4. The aforementioned patterns of pressure distribution increase with subsequent minutes of the CLE-test in the control subject.

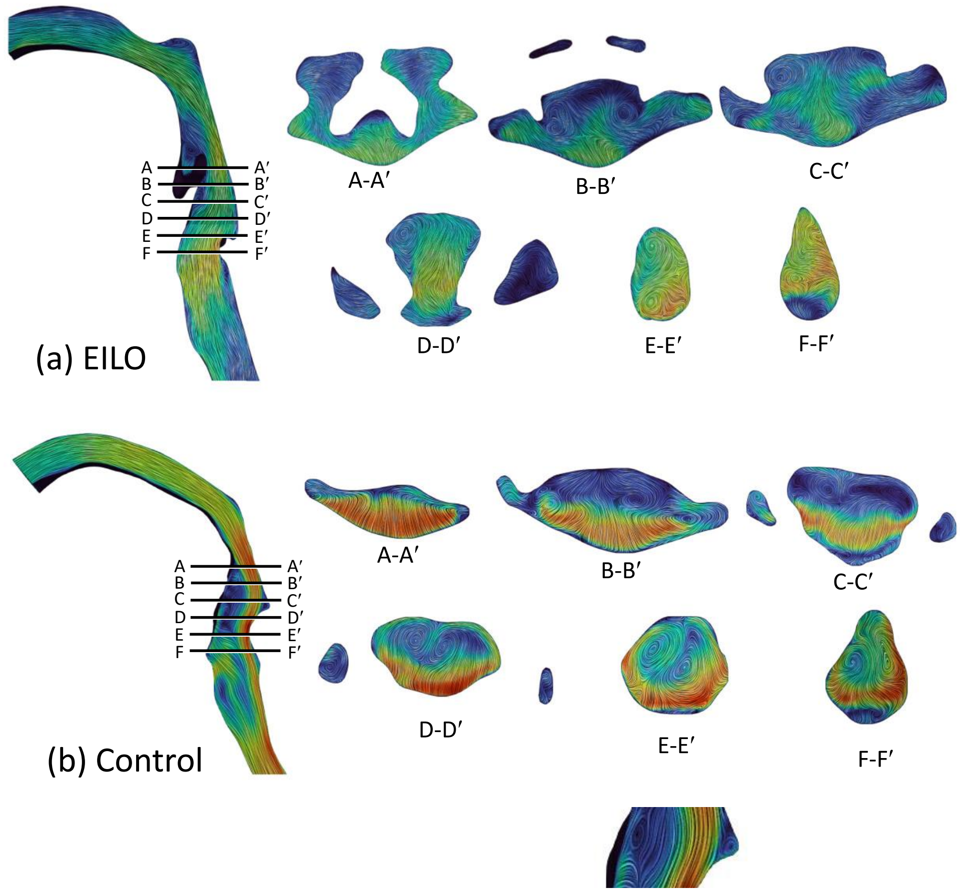

Figure 2. Mid-sagittal and axial cross-sections (A-A′ to F-F′) through the URT demonstrating normalised velocity magnitudes for the EILO (a) and control (b) participants. Axial cross-sections are arranged so that the anterior aspect is towards the top. Velocity is normalised with respect to the inlet velocity in all cases.

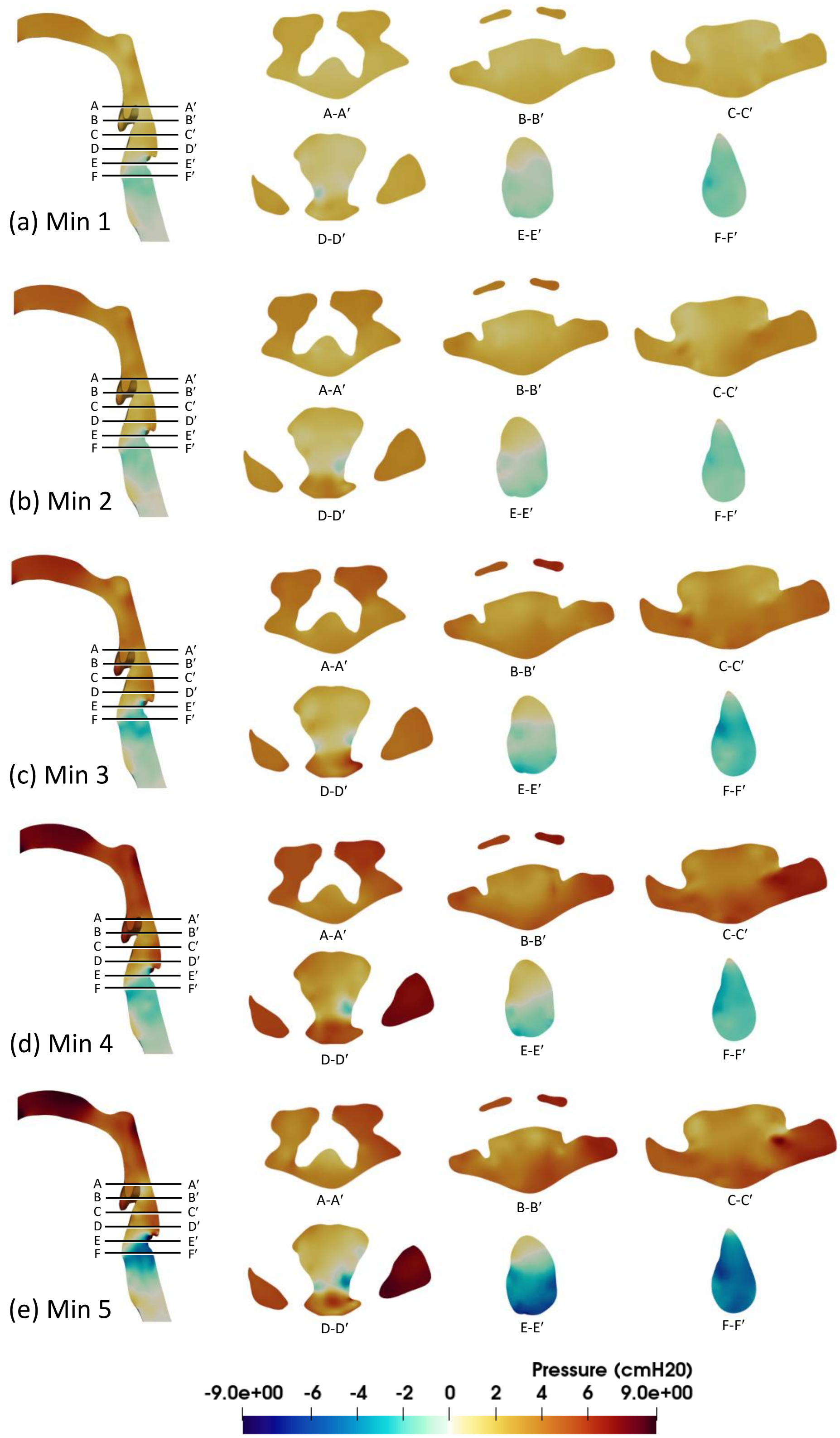

Figure 3. Mid-sagittal and axial cross-sections (A-A′ to F-F′) through the URT demonstrating air pressure field for the EILO subject. (a) – (e) correspond to the five minutes of the CLE-test. Axial cross-sections are arranged so that the anterior aspect is at the top.

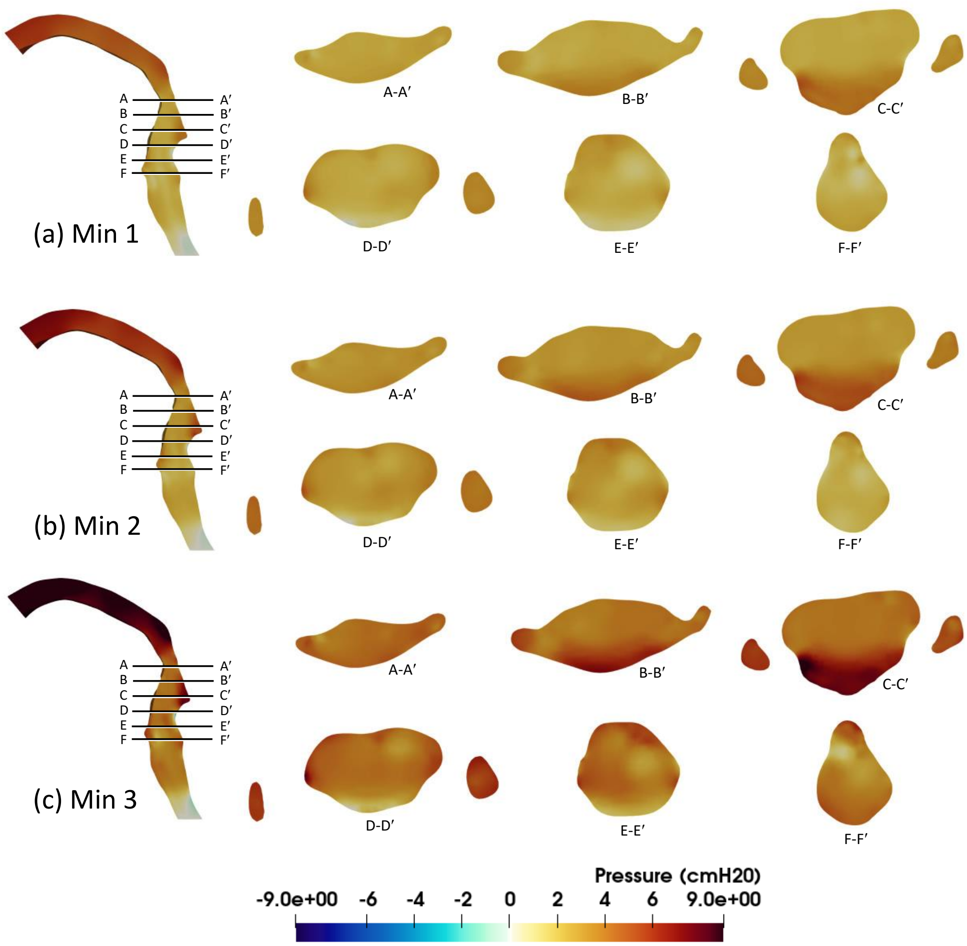

Figure 4. Mid-sagittal and axial cross-sections (A-A′ to F-F′) through the URT demonstrating relative changes in the air pressure field for the control subject. (a) – (c) correspond to the three minutes of the CLE-test. Axial cross-sections are arranged so that the anterior aspect is towards the top.

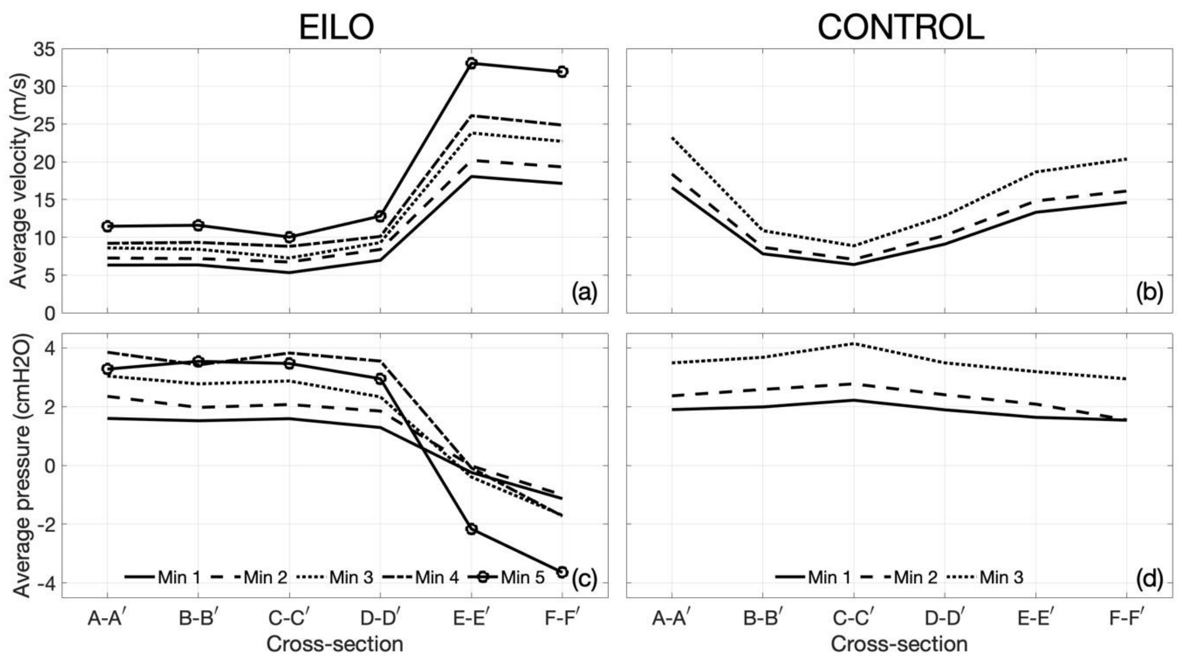

Figure 5. Average velocity (a,b) and pressure (c,d) over axial cross-sections at each flow rate for the control and EILO participants.

Average velocity and pressure value at supraglottic and hypopharyngeal cross-sections for both participants are shown in Figure 5. In the EILO subject, the average velocity through the upper supraglottis (A-A′ to D-D′) is consistent and is highest at E-E′ and F-F′ at the narrower glottis. The pressure in the supraglottis increases with higher initial flow rates across the minutes of CLE-test. However, variation is shown in the glottis where the pressure is similar until minute 5 where there is a significant drop in pressure. The control subject velocity values are higher in the epiglottic region (A-A′) due to a narrower cross-section in comparison to the EILO subject which subsequently slows in the upper supraglottis before increasing at the glottis, but not above the epiglottic values. The average pressures in the control subject are initially similar to the EILO subject but remain higher in the presence of increased velocity. Collectively, when comparing the velocity and pressure values across the minutes of the CLE-test – as the flow rates increase the velocities and pressures rise.

Comparison of the iso-ventilation condition

The participants used in the study achieved different airflow rates at maximal exercise. Therefore, it is pertinent to analyse the airflow and pressure behaviours between the participant geometries under the same airflow rate conditions. A simulation was conducted using the airflow rates in an iso-ventilation condition, shown in Table 2. A comparison of the CFD results in the iso-ventilation condition demonstrate no significant differences in terms of normalised velocity and wall pressure distributions from the results presented at true maximal exercise airflow rates. Therefore, analysis at peak exercise presents the most appropriate timepoint for comparison, due to the degree of laryngeal obstruction

Comparison of aerodynamic wall forces

Inspiratory force vectors induced by average inspiratory flow in the final minute of the CLE-test in the EILO and control subject are demonstrated in Figure 6. The EILO subject exhibited inwardly directed forces at both supraglottic and glottic regions, apart from the anterior most supraglottic region (SG1) which indicates a strong anteriorly directed force vector. The control subject demonstrated that all force vectors across the laryngeal airway were directed outward at all times, with little to no directional changes. Interestingly, differences emerge when comparing the supraglottic and glottic regions. Specifically, forces acting on the glottic wall show little variance in the direction of forces across different flow rates but increase in magnitude. While supraglottic force vectors were shown to exhibit variation in direction with some areas demonstrating nonlinear increases in force magnitude. Supraglottic regions SG2 and SG3 correspond to the areas that typically collapse inward and obstruct the airway in supraglottic-EILO. Figure 7 shows a detailed analysis of SG2 and SG3 in the EILO and control participants. In the EILO subject, the SG2 region shows quasi-linear increases in resultant force magnitude across the exercise test. Directional variations occur at minutes 4 and 5 as the force vector becomes directed towards the midline. These changes are also observed in forces acting on SG3, with the addition of a nonlinear increase in force magnitude on the right side. The inwardly directed force vectors shown in the EILO subject resemble the direction of collapse observed during the CLE-test (Figure 6). These findings are in contrast to the control subject where region SG2 and SG3 remain consistently directed outward with quasi-linear increases in force magnitude. The changes in dyspnoea intensity across the CLE-test align with the non-linear and linear increases of force exerted on SG2 and SG3.

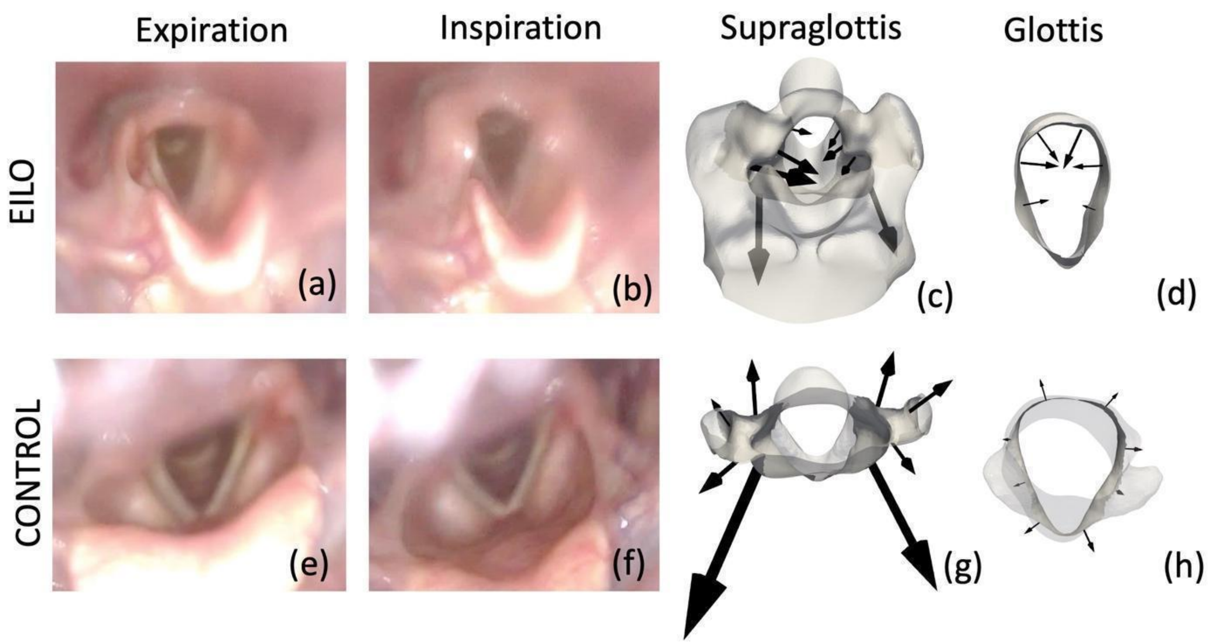

Figure 6. Laryngoscopic views and wall force vectors for the EILO (a-d) and control subject (e-f) in their final minute of CLE-test.

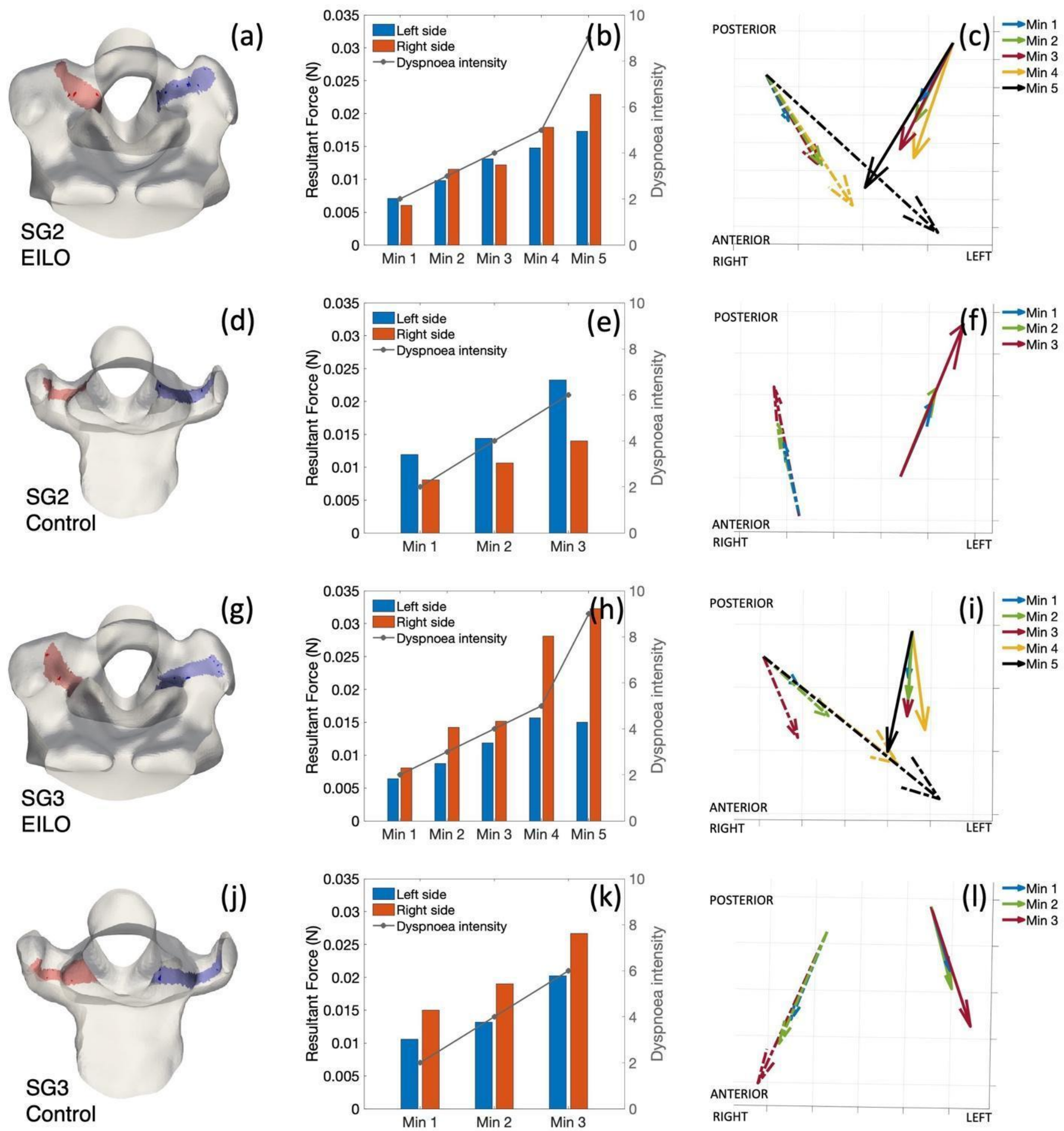

Figure 7. Air-induced force magnitude and direction for SG2 and SG3 in EILO and control participants. (a,d,g,j) Supraglottic regions of interest (SG2 and SG3) for the EILO and control participants. (b,e,h,k) Resultant force magnitudes for each minute of the CLE-test on the left (blue) and right (red) sides with dyspnoea intensity scores. (c,f,i,l) Direction of the resultant for vectors for each minute of the CLE-test on the left (solid arrow) and right (dashed arrow) sides.

DISCUSSION

The underlying pathophysiological mechanisms of EILO are poorly understood, due to its episodic nature and the difficulty in obtaining the necessary data in-vitro. An investigation of the mechanical insufficiency hypothesis in EILO requires an understanding of the aerodynamic forces experienced by patients with a comparison to healthy individuals. At present, there is a scarcity of approaches to investigate inspiratory airflow parameters in the laryngeal airway. The current study explores a novel hybrid methodological approach incorporating in-vitro exercise physiology and in-silico CFD modelling to investigate parameters that are otherwise inaccessible through in-vitro studies. CFD analysis permits global control of variables and facilitates the systematic testing of hypotheses pertaining to complex problems. In the current study, average inspiratory flow rate for each minute of the CLE-test was used to drive airflow through an accurate 3D reconstruction of the URT acquired from MRI scan data. Hence, the CFD simulations utilised different URT geometries and flow rates as variables in the analysis and comparisons between participants.

Fretheim-Kelly et al. [24] showed that translaryngeal airway resistance can be acquired through a two-point pressure measurement, where pressure transducers are placed at the pre-epiglottic and tracheal regions. This approach was shown to be well tolerated by exercising individuals with reasonable repeatability [24]. This method of two-point recording of pressure can quantify airway resistance between patient groups and provide a metric to monitor changes in patients over time. However, it does not capture high resolution pressure changes in the spatial domain that is necessary to understand the interaction of airflow with the surrounding anatomy. Therefore, the use of CFD analysis presents a valuable opportunity to quantify the temporal and spatial changes of laryngeal airflow and is a promising novel approach to analyse the pathophysiological mechanisms of EILO.

The key finding from this case series is that there is a significant disparity in the direction of force acting on the supraglottic walls between the EILO and control participants. The CFD model demonstrates that inspiratory airflow of the EILO subject exerts an inwardly directed force on the glottic and supraglottic walls, with the exception of the anterior most element of the supraglottis, as shown by Figure 6(c-d). This finding is matched to the supraglottic displacement observed endoscopically during the CLE-test, see Figure 6(a-b). In EILO, the supraglottic region is most susceptible to collapse, with or without concomitant closure of the glottis. The region of the posterior aryepiglottic folds and cuneiform cartilages exhibit the highest degree of inward deformation in supraglottic EILO and correspond to regions SG2 and SG3 the numerical simulations. Figure 7 shows a detailed analysis of these regions. It is found that as flow rate increases the magnitude of forces acting on the supraglottis increase asymmetrically and can demonstrate a nonlinear relationship as flow rates reach maximal exercise intensity. This relationship is evidenced when observing the right SG3 region in Figure 7 and corresponds to the endoscopically observed medial collapse of the supraglottic structures and the increase in dyspnoea intensity perceived by the EILO subject. It can also be seen that the direction of the force is consistent in minutes 1 to 3 of the CLE-test, which later become increasingly medialised by minute 5 with increase ventilation. The varying directionality of the force vectors may be explained by increased levels of turbulence and flow instability surrounding the aryepiglottic folds.

In the control subject, there are differences in force distribution of the laryngeal airway compared to the EILO subject, with all forces directed outward and little to no variation in direction. The magnitude of the resultant force vectors demonstrates a linear relationship with flow rate across the minutes analysed. While the model utilises two variables (geometry and flow rate) to make comparisons it is likely that the geometrical configuration is the predominant cause for the variation in the findings. When comparing the geometries of the two participants, there are notable differences in the reconstructed features of the URT airway between the two participants, such as the lack of space surrounding the epiglottis and the dimensions and shape of the piriform fossae. These anatomical features are known to elicit changes in laryngeal wall forces and may contribute to differences observed between participants.

Limitations and Future Directions

For the first time, it has been shown that a hybrid-approach combining CFD with current investigatory approaches into EILO can be used to approximate the magnitude and direction of aerodynamic forces. The outlined notable differences in the distribution and progression of forces that align with clinical observations in those with EILO should be confirmed in a larger sample. The findings suggest that a detailed analysis of geometric configurations of the airway is required to outline potential anatomical differences in EILO patients and how this may influence airflow. An understanding of this relationship would allow for further development of treatment and management options for clinicians encountering EILO. The CFD model used is limited by the URT airway having rigid walls, therefore, future work can explore incorporating the deformable characteristics of the airway to increase the fidelity of the model to in-vitro conditions.

The geometries used in the CFD model were acquired from a supine MRI scan at rest, due to the inability to acquire imaging and conduct the CLE-test simultaneously. This does not influence the CFD data comparisons, as imaging protocols were consistent between participants.

CONCLUSION

For the first time, airflow through the laryngeal airway of an EILO patient is analyzed by utilizing a hybrid approach that combines CFD and physiological data. Results of the computations reveal a significant disparity in the airflow and force distribution of the laryngeal airway between an EILO patient and a healthy matched control. Computations of the EILO patient demonstrate force vectors that aligns with obstruction observed during laryngoscopic visualisation and dyspnoea intensity during exercise. The current in-vivo methods for investigation into to the mechanisms of EILO are unable to obtain the highly detailed measurements of wall pressure to evaluate the influence of airflow on laryngeal collapse. The results from the hybrid-method shows great potential in calculating subject specific airflow forces during exercise. Therefore, can be used to further develop understanding of pathophysiological mechanisms of EILO. However, studies in larger sample sizes are now required to confirm these preliminary findings.

APPENDIX

Theory and numerical solution

The turbulent airflow in the URT is solved using Reynolds-averaged Navier-Stokes (RANS) equations for a homogenous, Newtonian and incompressible fluid, in a Cartesian coordinate system are given as:

$$\bar{u}_{i,i} = 0, \qquad i = 1, 2, 3 \tag{1}$$

$$\bar{u}_{j,t} + \left(\bar{u}_i\,\bar{u}_j + \overline{u_i' u_j'}\right)_{,i} = g_j - \frac{1}{\rho}\,\bar{p}_{,j} + \nu\bar{u}_{j,ii}, \qquad i, j = 1, 2, 3 \tag{2}$$

where ρ is the fluid density, ν is the kinematic viscosity, $\vec{g}$ is the gravitational acceleration, and p is the pressure gradient. $\vec{u}$ describes the velocity field, and $\vec{n}$ is the unit normal vectors in the i direction. F BAR is the time-averaged value of the fluctuating arbitrary variable f. The focus of the current study is to examine the air-induced force experience in the URT. The standard k-ω model for turbulence closure has been shown to accurately predict static wall pressures in the pharyngeal and laryngeal airway [23], and thus, is used in this model. The standard k-ω turbulence model relates kinematic viscosity to turbulence kinetic energy and dissipation by:

$$\nu_t = \frac{\rho k}{\omega}, \tag{3}$$

where, ν_t is the eddy viscosity, k is the turbulent kinetic energy and ω is the specific turbulence dissipation rate [22]. The simulations of airflow were performed using OpenFOAM (v2006), an open-source CFD package. The discretisation of the RANS equations was achieved using the finite volume method and was iteratively solved by the PIMPLE algorithm, for pressure-velocity coupling.

Numerical set-up

The boundary conditions used in the simulations are similar across all cases. A fixed pressure was set to 0 Pa at the outlet (trachea). At the inlet (mouth), a steady uniform volumetric flow rate (L/min) was applied to drive airflow. The flow rates used for each case are given in Table 2. The no-slip condition was applied to the rigid URT walls for all simulations. Fluid properties of ρ = 1.225 kg/m^3 and ν = 1.8 x 10^{-5} are used to represent air.

The subject geometries were meshed using snappyHexMesh to form a hex and split-hex grid of cells in the URT, consisting of 1,070,160 and 861,226 cells for the EILO-subject and control subject, respectively. A mesh convergence study for the current CFD model demonstrated less than 3% variation in pressure field values. Further detailed are presented by Reid et al. [18]. A Courant number < 0.5 was maintained by using a variable time-step condition and a residual convergence level of 1×10^{-5} is set for all variables. Simulations were conducted on two Intel Xeon E5-2697A v4 processors (16 cores, 3.00 GHz), and took between 47 h and 104 h of CPU time.

GLOSSARY

ω – turbulent specific energy

k – turbulent kinetic energy

ν – kinematic viscosity

ν_t – turbulent viscosity

ρ – fluid density

p - pressure

u – velocity

g – gravitational acceleration

ACKNOWLEDGMENTS

GRANTS

The work of JT, PL, and EW was funded by the Novo Nordisk grant to Team Denmark.

DISCLOSURES

The authors have no conflicts of interest.

AUTHOR CONTRIBUTIONS

LR - Conceived and designed research, performed computational simulations, analysed and interpreted data, prepared figures, drafted manuscript, edited and revised manuscript, approved final version of manuscript.

JT - Collected data, edited, and revised manuscript, approved final version of manuscript.

OJP - Analysed and interpreted data, provided input to figures, edited and revised manuscript, approved final version of manuscript.

MH - Conceived and designed research, analysed and interpreted data, provided input to figures, edited and revised manuscript, approved final version of manuscript.

LP - Edited and revised manuscript, approved final version of manuscript.

EW - Conceived and designed research, collected data, analysed and interpreted data, provided input to figures, edited and revised manuscript, approved final version of manuscript.

REFERENCES

[1] **Halvorsen T, Walsted ES, Bucca C, Bush A, Cantarella G, Friedrich G, Herth FJF, Hull JH, Jung H, Maat R, Nordang L, Remacle M, Rasmussen N, Wilson JA, Heimdal J-H.** Inducible laryngeal obstruction: an official joint European Respiratory Society and European Laryngological Society statement, *European Respiratory Journal*, 50: 1602221, 2017.

[2] **Price OJ, Walsted ES, Hull JH.** Understanding the total airway response to exercise: current perspectives and future challenges, *Current Opinion in Physiology, 10,* pp. 185-192. 2019.

[3] **Hall A, Thomas M, Sandhu G, Hull JH.** Exercise-induced laryngeal obstruction: a common and overlooked cause of exertional breathlessness. *British Journal of General Practice*, 66(650): e683-5. 2016.

[4] **Christensen PM, Thomsen SF, Rasmussen N, Backer V.** Exercise-induced laryngeal obstructions: Prevalence and symptoms in the general public, *European Archives of Oto-Rhino-Laryngology*, 268(9), pp. 1313–1319, 2011.

[5] **Sails J, Hull JH, Allen H, Darville L, Walsted ES, Price OJ.** High prevalence of exercise-induced stridor during Parkrun: a cross-sectional field-bases evaluation, *BMJ Open Respiratory Research, 7,* e000618. 2022.

[6] **Johansson H, Norlander, K, Berglund, L, Janson, C, Malinovschi, A, Nordvall, L, Nordang, L and Emtner, M.** Prevalence of exercise-induced bronchoconstriction and exercise-induced laryngeal obstruction in a general adolescent population, *Thorax*, 70(1), pp. 57–63, 2014.

[7] **Nielsen EW, Hull J, Backer V.** High prevalence of exercise-induced laryngeal obstruction in Athletes. *Medicine & Science in Sports & Exercise,* 45(1), pp. 2030-2035, 2013.

[8] **Walsted ES, Famokunwa B, Andersen L, Rubak SL, Buchvald F, Pedersen L, Dodd J, Backer V, Nielsen KG, Getzin A, Hull, JH.** Characteristics and impact of exercise-induced laryngeal obstruction: an international perspective, *ERJ Open Research*, 7(2), pp. 00195–02021, 2021.

[9] **Price OJ, Walsted ES, Bonini M, Brannan JD, Bougault V, Carlsen K-H, Couto M, Kippelen P, Moreira A, Pite H, Rukhadze M, Hull JH.** Diagnosis and management of allergy and respiratory disorders in sport: An EAACI task force position paper. *Allergy: European Journal of Allergy and Clinical Immunology, 77*(10), pp. 2909-2923, 2022.

[10] **Hull JH, Walsted ES, Pavitt MJ, Menzies-Gow A, Backer V, Sandhu G.** High Prevalence of Laryngeal Obstruction during Exercise in Severe Asthma. *American Journal of respiratory and Critical Care Medicine*, 199(4): 538-42. 2019.

[11] **Low K, Lau KK, Holmes P, Crossett M, Vallance N, Phyland D, Hamza K, Hamilton G, Bardin PG.** Abnormal vocal cord function in difficult-to-treat asthma. *American Journal of respiratory and Critical Care Medicine*, 184(1): 50-6. 2011.

[12] **Low K, Ruane L, Uddin N, Finlay P, Lau KK, Hamza K, Holmes PQ, Hamilton G, Bardin PG.** Abnormal vocal cord movement in patients with and without airway obstruction and asthma symptoms. *Clinical & Experimental Allergy*, 47(2): 200-7. 2017.

[13] **Baz M, Haji GS, Menzies-Gow A, Tanner RJ, Hopkinson NS, Polkey MI, Hull JH.** Dynamic laryngeal narrowing during exercise: a mechanism for generating intrinsic PEEP in COPD? *Thorax,* 70: 251-257. 2015

[14] **Walsted ES, Faisal A, Jolley CJ, Swanton LL, Pavitt MJ, Luo YM, Backer V, Polkey MI, Hull JH.** Increased respiratory neural drive and work of breathing in exercise-induced laryngeal obstruction, *Journal of Applied Physiology*, 124(2), pp. 356–363, 2018.

[15] **Riede T, Stein A, Baab KL, Hoxworth JM. (2023).** Post-pubertal developmental trajectories of laryngeal shape and size in humans. *Scientific Reports, 13,* 7673, 2023.

[16] Liu Y, Mitchell J, Chen Y, Yim W, Chu W, Wang RC. Study of the upper airway of obstructive sleep apnea patient using fluid structure interaction, *Respiratory Physiology and Neurobiology*, 249, pp. 54–61, 2018.

[17] Ye L, Wei J, Liang Z, Li Y, Wu M, Zhao C, Weng J, Liu X, SJ, Qu, S. Fluid dynamics of the upper airway in pediatric patients with severe laryngomalacia, *Physical and Engineering Sciences in Medicine*, 45(4), pp. 1083–1091, 2022.

[18] Reid L, Hayatdavoodi M, Majumdar S. Airflow through the supraglottis during inspiration. *Computer Methods in Biomechanics and Biomedical Engineering*, 26(12), pp. 1462–1477, 2023.

[19] Reid L, Hayatdavoodi M. Hypopharyngeal geometry impact on air-induced loads on the supraglottis, *Computer Methods in Biomechanics and Biomedical Engineering*, 2023. In press DOI: 10.1080/10255842.2023.2285723.

[20] Döllinger M, Jakubaß B, Cheng H, Carter SJ, Kniesburges S, Aidoo B, Lee CH, Milstein C, Patel RR. Computational fluid dynamics of upper airway aerodynamics for exercise-induced laryngeal obstruction: A feasibility study, *Laryngoscope Investigative Otolaryngology*, 8(5), pp. 1294–1303, 2023.

[21] Heimdal JH, Röksund OD, Halvorsen T, Skadberg BT, Olofsson J. Continuous laryngoscopy exercise test: A method for visualizing laryngeal dysfunction during exercise, *The Laryngoscope, 116*(1), pp. 52-57, 2009.

[22] Wilcox, DC. Turbulence modelling for CFD. La Canada: DCW Industries, Inc, 1998.

[23] Mylavarapu G, Murugappan S, Mihaescu M, Kalra M, Khosla S, Gutmark, E. Validation of computational fluid dynamics methodology used for human upper airway flow simulations, *Journal of Biomechanics*, 42(10), pp. 1553–1559, 2009.

[24] Fretheim-Kelly Z, Halvorsen T, Heimdal J, Strand E, Vollsæter M, Clemm H, Roksund O. Feasibility and tolerability of measuring translaryngeal pressure during exercise, *The Laryngoscope*, 129(12), pp. 2748–2753, 2019.